Climate Dynamics (2019) 53:1477–1495
https://doi.org/10.1007/s00382-019-04683-7

Planetary and synoptic-scale dynamic control of extreme cold wave patterns over the United States

Zuowei Xie[1] · **Robert X. Black**[2] · **Yi Deng**[2]

Received: 13 June 2018 / Accepted: 12 February 2019 / Published online: 21 February 2019

Abstract
The roles of planetary and synoptic-scale waves in extreme cold wave (ECW) events over the southeastern (SE) and northwestern (NW) United States (US) are studied using a spherical harmonic decomposition in conjunction with piecewise tendency diagnosis (PTD). Planetary waves and synoptic waves *jointly* work together to initiate ECW events. Notably, the planetary waves not only provide a direct contribution to circulation field enacting ECW events but also alter the background circulation field in such a manner that promotes synoptic waves growth via increases in regional barotropic deformation. The SE-ECW events, concurrent with the Northern Hemisphere annular mode (NAM) negative phase, feature high latitude intensification and subsequent southeastward movement of cold surface air temperature (SAT) anomalies. The planetary-scale pattern provides a sizable contribution to the total wave pattern on both sea level pressure (SLP) and upper level. Moreover, the negative NAM planetary anomaly acts to displace the jet equatorward and thereby increases the barotropic deformation of the synoptic-scale anomaly over southeastern US. PTD confirms that the planetary-scale barotropic deformation plays a key role in deepening the negative height anomaly with a secondary contribution from baroclinic growth. In contrast, NW-ECW events feature a regional SAT cold anomaly that intensified in situ in association with a quasi-stationary positive SLP anomaly with a substantial planetary-scale wave component. The upper level circulation is characterized by a pronounced anomalous ridge over the Gulf of Alaska and a northeast-southwest tilted negative height anomaly to its east. The negative height anomaly axis is orthogonal to the planetary-scale dilatation, result in a stronger planetary barotropic deformation of the incipient negative height anomaly.

Keywords Extreme cold wave · Large-scale meteorological pattern · Planetary wave · Barotropic deformation · Piecewise tendency diagnosis

1 Introduction

Extreme cold wave events (also denoted cold air outbreaks; both here referred to as ECWs), which are characterized by a rapid and intense air temperature drop, have profound societal and ecological consequences. The occurrence, intensity, spatial extent, and duration of ECWs have increased in association with recent climate change (IPCC 2012; Westby et al. 2013; Cohen et al. 2014; Trenary et al. 2015). Given their importance, the scientific study of ECWs has increased in recent scientific literature and government reports (e.g., IPCC 2012; Grotjahn et al. 2015), emphasizing long-term variability and links to planetary-scale climate modes such as El Niño Southern Oscillation, the Pacific Decadal oscillation and the North Atlantic Oscillation (NAO). Although a statistically significant modulation of the regional frequency of ECWs by major planetary-scale climate modes has been identified (e.g., Westby et al. 2013), it is additionally recognized that ECWs are more directly related to regional large-scale meteorological patterns (LMPs) than planetary-scale climate modes (Grotjahn et al. 2015; Xie et al. 2017a).

It is now well recognized that planetary-scale climate modes have a statistical impact upon ECWs as they preferentially modulate regional ECW frequency of over the US. For example, the negative NAO phase favors the occurrence of ECWs in the southeastern US, while the negative phase

✉ Zuowei Xie
xiezuowei@mail.iap.ac.cn

[1] International Center for Climate and Environment Sciences, Institute of Atmospheric Physics, Chinese Academy of Sciences, Beijing 100029, China

[2] School of Earth and Atmospheric Sciences, Georgia Institute of Technology, Atlanta 30332, GA, USA

of Pacific-North American (PNA) teleconnection pattern favors the occurrence of ECWs over the western US (Walsh et al. 2001; Cellitti et al. 2006; Westby et al. 2013; Westby and Black 2015). Thompson and Wallace (1998) illustrated that the so-called Arctic Oscillation (AO) encompasses the NAO but with a broader horizontal scale and higher degree of zonal symmetry, and thus accounts for a considerably larger fraction of the Northern Hemisphere SAT variance. The tropospheric signature of the AO, known as the Northern Hemisphere annular mode (NAM), extends from the surface upward into the stratosphere (Thompson and Wallace 1998; McDaniel and Black 2005). Kolstad et al. (2010) investigated the relationship between stratospheric weak vortex events and ECWs using reanalysis data and a set of coupled climate models. They noted that the weakest vortex phases can increase the probability of ECWs over the east coast of North America by 50% via the influence of the troposphere NAM. Xie et al. (2017b) identified six boreal cold season daily planetary wave patterns using spherical harmonic analysis. They found that one pattern resembling the negative NAM phase and a second combining the negative West Pacific (WP) teleconnection and positive NAO phases both favor the occurrence of ECWs over the continental US. Baxter and Nigam (2015) demonstrated that, during the winter of 2013/2014, the North Pacific Oscillation-WP teleconnection provided a major contribution to the North American circulation anomaly. Harnik et al. (2016) discovered that a large number of extreme North American cold events are related to jet stream undulations similar to the circumglobal North America pattern (Branstator 2002). Although the statistical significance between planetary climate modes and seasonal ECW behavior is well established, little information exists regarding the *intraseasonal* links between planetary climate modes and ECWs or the underlying physics behind these relationships.

As discussed above, regional-scale LMPs provide a more direct influence upon ECWs and, since they are also modulated by planetary-scale climate modes (Grotjahn et al. 2015), represent a physical pathway between climate modes and ECWs. Konrad and Colucci (1989) pointed out that ECWs develop in response to the propagation of synoptic scale waves through a longwave trough positioned near the east coast of North America. Konrad (1996) examined the relationship between ECWs and planetary- and synoptic scale circulation features and found that planetary-scale anomalies are more strongly related to ECW intensity than synoptic-scale anomalies. Furthermore, Konrad (1998) compared the relation between ECW intensity and mean planetary scale circulation at 5, 10 and 15 days and found that intense ECWs tend to be associated with the 10- and 15-day mean circulation. Walsh et al. (2001) showed that ECWs over the US feature a positive Arctic sea level pressure anomaly generally displaced geographically with respect to the nodal locations of the NAO and AO. Specifically, a positive Arctic sea level pressure anomaly center detaches and migrates southeastward for ECWs over the East and Gulf coasts of the US, while the feature remains over northwestern North America for the ECWs over the Midwest US. Loikith and Broccoli (2012, 2014) examined LMPs and planetary-scale climate modes in relation to the occurrence of ECWs and noted that LMPs can overlap with planetary-scale climate modes, e.g., the negative NAM phase. Watt-Meyer and Kushner (2015) decomposed daily circulation anomalies for the 2013/2014 and 2014/2015 winter seasons into standing and travelling components using a two dimensional Fourier transform. Their results suggest that a mobile LMP contributed substantially to the ridge-trough dipole in 2013/2014, while the mobile synoptic contributions to the dipole were notably smaller in 2014/2015. Xie et al. (2017a) identified three distinct ECW patterns centered over the upper Midwest (UM), Northwest (NW) and Southeast (SE) US, respectively, along with associated LMPs. The LMPs, containing both planetary and synoptic wave features, bear some resemblance to the NAM-like, WP and NAO-like daily planetary patterns identified in Xie et al. (2017b). Given the above noted distinct roles of planetary and synoptic scale waves, there is a need to provide a more comprehensive examination of the respective contributions of daily planetary and synoptic scale component toward the LMPs responsible for ECWs.

Planetary waves act to modulate the structure of synoptic waves (Mak and Cai 1989; Black and Dole 2000). Zeng (1983) and Mak and Cai (1989) illustrated that the barotropic development of an isolated disturbance will occur if it has a favorable structural orientation in relation to the planetary flow. A disturbance that is locally elongated along the axis of contraction (dilation) of the background deformation field will barotropically grow (decay). Black and Dole (2000) discovered that the strongest barotropic stretching deformation is found in the mid-latitude jet entrance (zonal dilatation) and exit (meridional dilatation) regions. Thus, a transient eddy with an initially isotropic horizontal shape will tend to become zonally (meridionally) elongated within the jet entrance (exit) regions. Nielsen-Gammon and Lefevre (1996) developed the piecewise tendency diagnosis (PTD) based on the advective conservation of quasigeostrophic potential vorticity (PV). PTD distinguishes among Rossby wave propagation, baroclinic and barotropic growth and wave–wave interaction. Nielsen-Gammon and Lefevre (1996) applied PTD to explore the dynamical evolution of a small-scale upper-level trough embedded within a large-scale flow. They found that the mobile trough is initiated by Rossby wave energy from upstream disturbances over the northwest Pacific, which induce a strong asymmetrical structure in the incipient trough. As the trough develops, it

helps to promote the growth of a surface cyclone, which in turn amplifies the trough via a westward tilt and baroclinic growth. Nakamura et al. (1997), using a different set of dynamic diagnostic tools, found that the high- and low-frequency waves play different roles in European and North Pacific blocking, respectively. Messori et al. (2016) found that the ECWs over the southeast US are associated with southward cold air advection, which leads to a highly baroclinic environment by enhancing the land-sea contrast on the eastern seaboard of North America, promoting an intense quasi-stationary upper cyclone circulation. Evans and Black (2003) extended PTD to incorporate spherical geometry, diabatic heating and ageostrophic effects and identified the primary growth mechanisms responsible for persistent flow anomalies. They found that barotropic deformation, baroclinic growth and nonlinear eddy feedback play different roles in the various categories of persistent flow anomalies occurring over the North Pacific and North Atlantic. Jiang et al. (2013) showed that the interaction between high-frequency (2–6 day periods) and intermediate-frequency (7–29 day periods) eddies acts as a sink for high-frequency eddy activity and a primary source of intermediate-frequency eddy activity. Francis and Vavrus (2012, 2015) showed that a weakened midlatitude jet leads to more frequent recurrent high-amplitude (wavy) configurations that favor persistent extreme weather patterns. Given the different roles of physical mechanisms for the various circulation components, further research is required to more fully characterize the dynamic mechanisms leading to the LMPs associated with ECW events.

In the current study, we focus on the life cycles of SE-ECW and NW-ECW events, which are related to a (a) negative NAM-like pattern and (b) combination of negative WP and positive NAO-like patterns, respectively. A spherical harmonic decomposition is applied to separate the anomalous circulation into planetary and synoptic-scale components to examine their respective roles in the dynamic evolution of ECW events. The linkages among upper tropospheric planetary and synoptic-scale circulations and near surface wind are investigated using piecewise potential vorticity inversion. We extend the PTD methodology of Evans and Black (2003) to account for the interaction between planetary scale and synoptic scale waves in quantitatively evaluating the contribution of different dynamic development mechanisms to LMPs. In the following section, we describe the data and methodology. Section 3 reviews the lifecycle of the SE-ECW events and related dynamic features. Section 4 presents the development characteristics and dynamic features of the NW-ECW events (with a comparison to the SE-ECW events). A summary and discussion are provided in the final section.

2 Data and methodology

In the current study, we use 6 hourly and daily reanalysis data provided by the National Centers for Environmental Prediction-National Center for Atmospheric Research Reanalysis (Kalnay et al. 1996) for 55 cool seasons (November 1st to March 31) during the period 1950–2005. The field variables considered are 2 m surface air temperature (SAT), sea level pressure (SLP), geopotential height, and horizontal winds. Surface data are provided in a T62 Gaussian grid with 194×94 points, while multilevel fields are on a 2.5°×2.5° latitude/longitude grid. The annual cycle is obtained by first averaging the 6 hourly and daily reanalysis data over all years (for each calendar day/hour) and then smoothing (to remove residual high-frequency variability) by only retaining the leading six annual Fourier harmonics of the resulting annual cycle. The 6 hourly and daily anomalies are obtained by subtracting the smoothed annual cycle from the original data at each grid point.

ECW events are identified in the same manner of Xie et al. (2017a) by isolating days when the daily SAT anomaly is below −1.5 standard deviations for at least 10% of the grid points over the continental US. ECW events are required to last at least three consecutive days and must be separated from one another by at least 8 days. The peak day is defined as the day with the most extensive cold SAT anomaly and is denoted day 0. Then, three ECW clusters are identified in applying agglomerative hierarchical clustering to the normalized SAT anomaly fields over the conterminous US. Considering the resulting cold SAT anomaly patterns, the three ECW clusters are denoted the upper midwest (UM), northwestern (NW) and southeastern (SE) ECW clusters, respectively. Finally, the original ECW events are categorized into respective clusters according to the cluster index occurring on Day 0.

To separate the planetary and synoptic-scale waves, a spherical harmonic analysis, two-dimensional spatial filter, is adopted in this study (Xie et al. 2017b). As in Xie et al. (2017b), a distribution of meteorological fields symmetric about the equator is assumed in order to highlight the Northern Hemisphere circulation. Using a triangular truncation, planetary wave features are taken to be wavenumbers 1–5, while wavenumbers 6 and greater are considered synoptic waves. It should be noted that, within this decomposition, wavenumber 0 represents the areal mean. Six distinct planetary wave patterns are identified by applying agglomerative hierarchical clustering to the daily *planetary* 500 hPa geopotential height (Z500) field over the Northern Hemisphere.

Horizontal quasi-stationary Rossby wave propagation is diagnosed using the wave-activity flux of Takaya and Nakamura (2001):

$$W = \frac{p}{2000|U|}\begin{bmatrix} u\left(v'^2 - \psi' v'_x\right) + v\left(-u'v' + \psi' u'_x\right) \\ u\left(-u'v' + \psi' u'_x\right) + v\left(u'^2 + \psi' v'_y\right) \end{bmatrix}, \quad (1)$$

where ψ'denotes perturbation geostrophic stream function, $\boldsymbol{u}' = (u', v')$ perturbation geostrophic wind velocity, $\boldsymbol{U} = (U, V)$ a basic state horizontal flow velocity, and p is pressure normalized by 1000 hPa. The basic state flow is taken to be the cool-season climatological average. For each ECW, daily perturbation values are obtained by removing the corresponding daily climatological mean value.

We apply the dilatation axis described by Mak and Cai (1989) and Black and Dole (2000), defined in terms of the barotropic deformation pseudovector D. The zonal and meridional components of D are expressed as:

$$D_1 = U_x - V_y, \tag{2a}$$

$$D_2 = V_x + U_y, \tag{2b}$$

Where the magnitude of the deformation pseudovector or dilatation is given by

$$D = \left(D_1{}^2 + D_2{}^2\right)^{1/2}, \tag{3}$$

And the angle of the dilatation relative to the zonal axis is given by

$$\theta = \frac{1}{2}\tan^{-1}\left(\frac{D_2}{D_1}\right), \tag{4}$$

To investigate the dynamical interaction between the planetary waves and synoptic waves, we employ the PTD method used by Nielsen-Gammon and Lefevre (1996) and Evans and Black (2003). We use the quasigeostrophic formulation in spherical geometry as derived by Evans and Black (2003) and expressed as:

$$\frac{\partial \Phi}{\partial t} = \mathcal{L}^{-1}\left(\frac{\partial q}{\partial t}\right) = \mathcal{L}^{-1}\left(-V \cdot \nabla q + S_H + S_{AG}\right), \tag{5}$$

where

$$q = f + \frac{1}{f}\frac{\partial^2 \Phi}{\partial x^2} + \frac{1}{f}\frac{\partial^2 \Phi}{\partial y^2} + f\frac{\partial}{\partial p}\left(\frac{1}{\sigma_p}\frac{\partial \Phi}{\partial p}\right), \tag{6}$$

is quasigeostrophic PV in spherical Coordinates, V is geostrophic velocity and

$$S_H = f\frac{\partial}{\partial p}\left(\frac{-QR}{\sigma_p p}\right),$$

$$S_{AG} = -D_a q - D_g \xi_a + \xi_a \frac{\partial \omega_0}{\partial p} + \frac{v q_t}{f}\frac{df}{dy} - \frac{f}{\left(\theta_{ref}\right)_p}\left(\frac{\partial \theta'}{\partial x}\frac{\partial u_a}{\partial p} + \frac{\partial \theta'}{\partial y}\frac{\partial v_a}{\partial p}\right)$$
$$-\omega_0 \frac{\partial q}{\partial p} - f\frac{\partial \omega_0}{\partial p}\frac{\left(\theta'\right)_p}{\left(\theta_{ref}\right)_p} + f\omega_0 \frac{\partial}{\partial p}\left\{\theta' \frac{\partial}{\partial p}\left[\frac{1}{\left(\theta_{ref}\right)_p}\right]\right\} - \frac{\partial \omega_0}{\partial x}\frac{\partial v_g}{\partial p} + \frac{\partial u_g}{\partial p}\frac{\partial \omega_0}{\partial y}. \tag{7}$$

The term $\sigma_p = -(R/p)\left(p/p_s\right)^{\kappa}\left(d\theta_{rdf}/dp\right)$ is static stability, Q is diabatic heating, and θ is the potential temperature. The frictional force is taken to be small and is formally omitted here.

Similar to Nielsen-Gammon and Lefevre (1996), we adopt a spherical harmonic analysis to partition the total flow into a planetary-scale background environment encompassing a synoptic-scale perturbation. The planetary and synoptic components of the flow field are designated using the subscripts p and s, respectively:

$$V = V_p + V_s, \tag{8a}$$

$$q = q_p + q_s, \tag{8b}$$

substituting into (5),

$$\frac{\partial \Phi}{\partial t} = \mathcal{L}^{-1}\left(-V_s \cdot \nabla q_p - V_p \cdot \nabla q_s - V_s \cdot \nabla q_s - V_p \cdot \nabla q_p + S_H + S_{AG}\right). \tag{9}$$

When climatological-mean balance of (9) is subtracted, it becomes

$$\frac{\partial \Phi'}{\partial t} = \mathcal{L}^{-1}\begin{bmatrix}\left(-V_s \cdot \nabla q_p - \overline{V_s \cdot \nabla q_p}\right) + \left(-V_p \cdot \nabla q_s + \overline{V_p \cdot \nabla q_s}\right) + \left(-V_s \cdot \nabla q_s + \overline{V_s \cdot \nabla q_s}\right) \\ +\left(-V_p \cdot \nabla q_p + \overline{V_p \cdot \nabla q_p}\right) + S'_H + S'_{AG}\end{bmatrix}. \tag{10}$$

As in Nielsen-Gammon and Lefevre (1996) and Evans and Black (2003), partitioning the synoptic-scale wind field into separate parts induced by upper- (U = 500–100 hPa) and lower level (L = 1000–600 hPa) PV anomaly fields gives

$$\frac{\partial \Phi'}{\partial t} = \mathcal{L}^{-1}\left[\begin{array}{l}\underbrace{\left(-V_{sU}\cdot\nabla q_p - \overline{V_{sU}\cdot\nabla q_p}\right)}_{A} + \underbrace{\left(-V_{sL}\cdot\nabla q_p - \overline{V_{sL}\cdot\nabla q_p}\right)}_{B} + \underbrace{\left(-V_p\cdot\nabla q_s + \overline{V_p\cdot\nabla q_s}\right)}_{C} \\ + \underbrace{\left(-V_s\cdot\nabla q_s + \overline{V_s\cdot\nabla q_s}\right)}_{D} + \underbrace{\left(-V_p\cdot\nabla q_p + \overline{V_p\cdot\nabla q_p}\right)}_{P} + \underbrace{S'_H}_{E} + \underbrace{S'_{AG}}_{F-N}\end{array}\right]. \quad (11)$$

Partitioning Eq. (11) in this way relates local height anomaly changes to interactions between planetary waves and synoptic waves (terms A, B and C), nonlinear geostrophic advection (terms D and P), diabatic heating anomalies (term E) and several ageostrophic forcings. As Evans and Black (2003), we assess the 300 hPa geopotential height tendency from the advective and nonadvective PV sources/sinks only at levels within a 500–200 hPa layer. Following Nielsen-Gammon and Lefevre (1996) and Evans and Black (2003), Term A represent upstream wave propagation associated with the upper-level synoptic Rossby wave advecting the planetary PV gradient. Term B represents changes in the upper-level PV anomaly due to the influence of lower-level synoptic PV anomalies, thereby encompassing baroclinic growth. Term C is the advection of the synoptic PV anomaly wave pattern by the planetary geostrophic flow, including horizontal translation and the impact of horizontal and vertical deformation of PV anomalies by the planetary scale flow. Thus, Term C encompasses barotropic growth processes.

Given that diabatic heating is not directly available from the NCEP/NCAR reanalysis, we use the apparent heat source defined by Yanai et al. (1992):

$$Q = c_p\left(\frac{p}{p_0}\right)^{\kappa}\left(\frac{\partial\theta}{\partial t} + v\cdot\nabla\theta + \omega\frac{\partial\theta}{\partial p}\right), \quad (12)$$

where v is the horizontal velocity and ω is the vertical pressure velocity. In Eq. (12), $\kappa = R/c_P$, where R and c_p are the gas constant and specific heat at constant pressure of dry air, respectively. P_0 is 1000 hPa.

Following Nakamura et al. (1997), before compositing each anomaly field is horizontally translated in order to sharpen the coherent signals among individual events. In this translation, the entire field is shifted along a great circle that connects the negative anomaly center and the reference point is determined as the location of the composite negative anomaly center for Day 0 prior to performing translation. The composite signatures generally maintain their geographical structural identity as the translation procedure shifts each field by less than 500 km, a distance that is much smaller than the spatial scale of the negative height anomaly pattern. For each ECW event, the same lateral translation is applied to all the field variables at each level for each time lag relative to Day 0. A Student's t test is applied to the composite anomaly fields to assess the statistical significance (Wilks 2006).

3 Composite intraseasonal evolution of ECW events

3.1 The SE-ECW and NW-ECW Events

Figure 1 shows the composite circulation features for SE-ECW and NW-ECW clusters and associated planetary wave patterns (replotted from Xie et al. 2017a, b). Given that the circulation features are strongly asymmetric between the SE- and NW-ECW clusters, we focus on these two clusters in current paper. The mature SE-ECW structure shows cold SAT anomalies dominating the entire eastern US and southeastern Canada with a significant impact on the southeastern US (Fig. 1a). Northerly surface wind anomalies are mainly concentrated over eastern North America. In the mid troposphere, the associated LMP consists of a zonal wave train of height anomalies extending from the North Pacific eastward through the US into the North Atlantic, including a conspicuous negative height anomaly over the eastern US (Fig. 1c). Robust eastward Rossby wave energy propagation extends from the negative height anomaly, indicative of locally forced feature. The corresponding NW-ECW pattern is largely antisymmetric with respect to SE-ECW. Forced via the cold advection of anomalous northerly flow, a cold SAT anomaly prevails over the northwest and western coast of US with the strongest signature over the northern Rocky Mountains (Fig. 1b). The LMP features a quasi-zonal wave train of height anomalies extending eastward from the Gulf of Alaska, with a deep negative height anomaly feature over the Rocky Mountains (Fig. 1d). A Rossby wave energy flux directed toward the negative height anomaly is more evident than for SE-ECW events, suggesting that the negative anomaly is, at least in part, remotely forced.

Xie et al. (2017b) found that US ECW frequency is enhanced during episodes of the fourth and sixth planetary wave patterns identified in their study. To better quantify their connection to conventional teleconnection patterns, we calculate spatial correlation coefficients between the planetary wave patterns and several conventional teleconnection patterns, the latter obtained by regressing monthly mean Z500 anomalies against monthly teleconnection indices including AO, WP, PNA, East Pacific-North Pacific, Polar/Eurasia, East Atlantic and Scandinavia from the NOAA Climate Prediction Center (or CPC, http://www.cpc.ncep.noaa.gov/data/teledoc/telecontents.shtml). The pattern correlation results indicate that the fourth planetary wave pattern is closely related to the negative phase of NAM/AO with a correlation coefficient of −0.74 over the northern hemisphere. Considering their sixth pattern, the closest historical patterns are the negative phase of the WP (correlation coefficient of −0.81 over the North Pacific) and the positive phase of the NAO (correlation coefficient

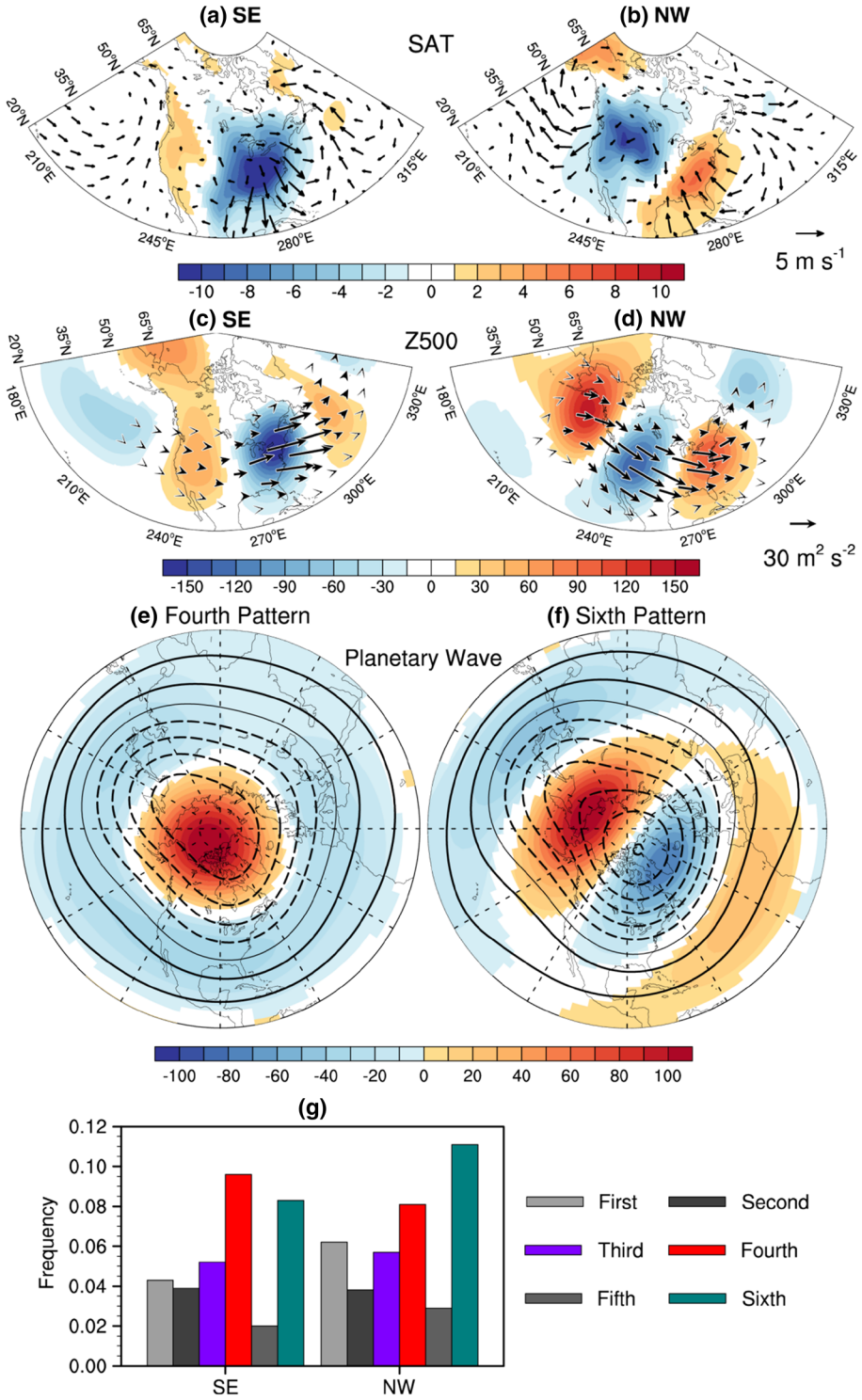

Fig. 1 Composite SAT anomalies (shaded; K) and surface horizontal wind anomalies (arrows, m s^{-1}) of **a** SE- and **b** NW-ECW groups, replotted from Fig. 3a, b in Xie et al. 2017a. Composite 500 hPa geopotential height (Z500) anomalies (shaded) and wave activity fluxes (arrows, units of m^2 s^{-2}) of **c** SE- and **d** NW-ECW groups, replotted from Fig. 5a, b in Xie et al. 2017a. Composite Z500 of wave 1–5 (contours) and corresponding anomalies relative to the climatological mean (shaded) for the **e** fourth and **f** sixth planetary wave pattern, adopted from Fig. 2e, f in Xie et al. 2017b. Only composite anomalies that are statistically significant at 95% confidence are shaded. **g** The frequency of two ECW groups during days concurrent with different planetary wave patterns

of −0.62 over the North Atlantic) (Fig. 1e, f). In comparison with prior studies (e.g., Konrad 1996; Thompson and Wallace 1998), the planetary waves in current paper are defined in terms of the *daily* Z500 structure restricted to wavenumbers 1–5 via a two-dimension spherical harmonic analysis as opposed to time filtering or averaging. To examine the relationship between each ECW group and the planetary wave patterns, Fig. 1g displays the occurrence frequency of ECWs, stratified in terms of the six planetary wave patterns identified by Xie et al. (2017b). Here, frequency is defined (separately for each planetary wave pattern) as the ratio of (a) days during which a specific ECW class and planetary wave pattern coincide to (b) the total number of days populated by the planetary

Table 1 Discrete event dates for SE-ECW events

	Period	Peak date	Duration
1	29 January–6 February 1996	3 February	9
2	16–31 December 1983	24 December	16
3	29 December 1969–10 January 1970	8 January	13
4	17–26 March 2002	22 March	10
5	19–22 January 1985	20 January	4
6	31 January–7 February 1988	6 February	8
7	26 February–6 March 1978	4 March	9
8	24–28 March 2001	26 March	5
9	22–25 January 2003	23 January	4
10	21–24 February 1968	22 February	4
11	24–29 January 1961	25 January	6
12	15–19 January 1977	17 January	5
13	28 January–1 February 1977	29 January	5
14	21–23 December 1960	22 December	3
15	11–14 March 1960	12 March	4
16	17–26 December 2000	22 December	10
17	2–10 March 2003	10 March	9
18	23–25 March 1971	24 March	3
19	15–23 February 1966	20 February	9
20	8–10 March 1984	9 March	3
21	6–8 February 1977	6 February	3
22	30 December 2000–3 January 2001	2 January	5
23	12–15 February 2004	15 February	4
24	28–31 January1965	31 January	4

Table 2 Discrete event dates for NW-ECW events

	Period	Peak date	Duration
1	29–31 December 1990	30 December	3
2	1–9 November 2003	5 November	9
3	28–31 March 1954	30 March	4
4	6–8 December1956	7 December	3
5	2–5 January 1960	3 January	4
6	22–24 November 1982	24 November	3
7	24–30 January 1957	29 January	7
8	23–27 March 1964	25 March	5
9	30 January–4 February 1956	1 February	6
10	23–25 March 1990	23 March	3
11	28–30 November 1975	30 November	3
12	20–22 January 1954	21 January	3
13	10–14 November 1979	10 November	5
14	7–10 March 2002	8 March	4
15	7–9 January 1980	8 January	3

wave pattern. We note that SE-ECWs are typically favored during episodes of the fourth pattern, while NW-ECWs are most frequent in association with the sixth pattern. To further explore the dynamic nature of the relationship between planetary wave patterns and ECW events, we identify for further study 24 SE-ECW events concurrent with the fourth planetary wave pattern and 15 NW-ECW events concurrent with the sixth pattern for periods of at least 3 days (Tables 1, 2).

3.2 The SE-ECW events

Figure 2 displays the composite evolution of SAT anomalies for the SE-ECW events. At day −4 (Fig. 2a), a modest cold anomaly extends over most of North America with the largest amplitudes to the lee of the Canadian Rockies. Meanwhile, a moderate northerly wind anomaly is observed over northwestern Canada. From day −2 to 0 (Fig. 2b, c), the cold SAT anomaly intensifies and is transported into the southeastern US. This coincides with the amplification of a north-northwest wind anomaly extending from the lee side of the Rockies to the southeastern US, serving to transport the cold air mass into the southeastern US. By day 2 (Fig. 2d), both the cold anomalies and northerly wind anomalies have considerably weakened. The SAT anomaly pattern and evolution generally correspond to the behavior identified by Westby and Black (2015), but with a stronger amplitude and broader areal coverage. We note that in Westby and Black (2015) SE-ECW events are defined in terms of the mean SAT anomaly within a 10° × 7.5° box over the southeastern US, but does not require all 24 grid points to be extreme simultaneously. In contrast, the methods applied in the current paper require that, for each ECW event, at least 10% of 237 US grid points (i.e., ~24 grid points) considered will be simultaneously characterized by SAT anomaly values below −1.5 standard deviation.

Figure 3 shows the composite life cycle of SLP anomalies for the SE-ECW events. At day −4 (Fig. 3a) the SLP anomaly pattern is characterized by significant high pressure extending from the Arctic to North America straddled by two low pressure features over the North Pacific and North Atlantic, respectively. The positive anomaly is located nearby and to the west of the cold SAT anomaly center (Fig. 2a). From day −2 to 0 (Fig. 3b, c), the high pressure feature extends southward through the continental US with the highest amplitude signature along the lee side of the Rockies. Meanwhile, a negative height anomaly over the Labrador peninsular magnifies and extends southward along the US coastline. The couplet of positive and negative SLP anomalies results in a pronounced anomalous northerly flow leading to a broad swath of cold advection. By day 2 (Fig. 3d), the positive SLP anomaly progresses into the southeastern US, has weakened considerably and has become detached from the Arctic high pressure feature, leading to ECW decay. To assess the contribution of planetary and synoptic-scale components, we decompose the

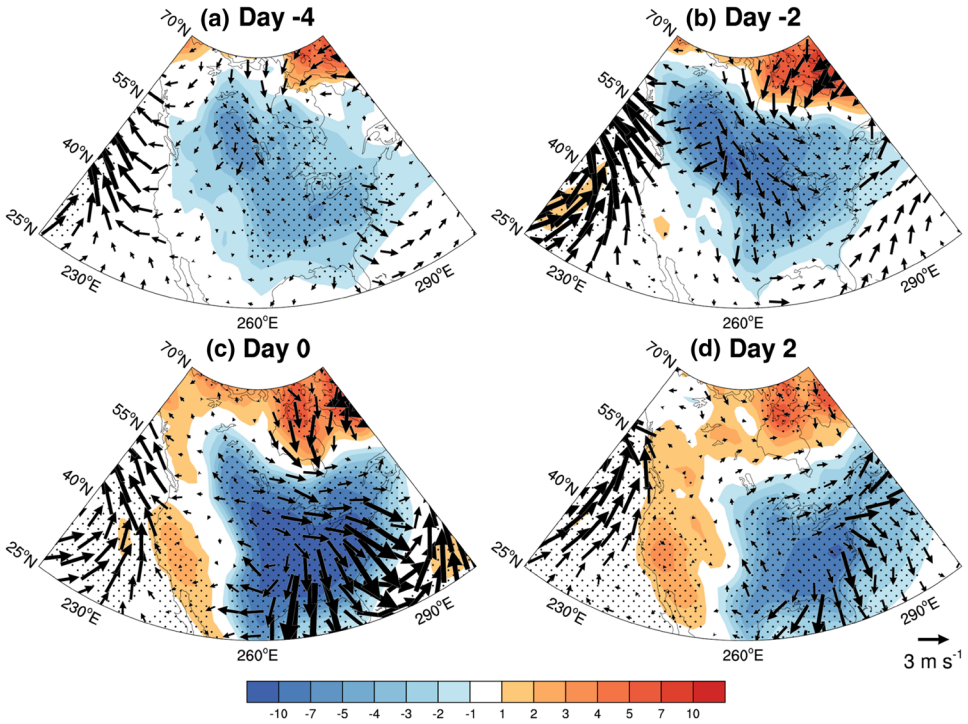

Fig. 2 Composite evolution of SAT anomaly (shaded, K) and surface wind anomaly (arrow, m s^{-1}) for the SE-ECW events. In all plots, the stippling indicates composite values that are significant at the 95% confidence level

SLP anomaly field into wave numbers 1–5 (planetary scales) and wave numbers greater than 6 (synoptic scales). Considering the planetary scale pattern (Fig. 3e–h), we note that it encapsules a broader negative anomaly feature extending from the North Atlantic to the east coast of North America. Therefore, the planetary wave structure partly resembles the negative phase of the AO (Thompson and Wallace 1998). Though the positive anomaly feature extends southward over the US by Day 0 (Fig. 3g), the amplitude is relatively weak compared to the respective total anomaly field, suggesting only a small contribution from the planetary wave. In contrast, prior to onset the synoptic-scale anomaly pattern consists of a zonal wave train extending from the North Pacific across North America to the North Atlantic leading to an east–west anomaly dipole over North America (Fig. 3i–l). The associated high pressure feature gradually amplifies and propagates southeastward from eastern Alaska between day −4 and 0, in concert with the southward outbreak of cold air from Canada.

Figure 4 displays the composite evolution of 300-hPa geopotential height (Z300) anomalies for SE-ECW events, spatially decomposed in the same manner as SLP. At day −4 (Fig. 4a) the total anomaly pattern includes a significant positive feature extending from the Arctic southward to the eastern North Pacific with two weaker, zonally elongated negative anomaly centers located, respectively, over the North Pacific and east-central North America through the North Atlantic. This pattern is associated with Rossby wave energy propagation from the Pacific negative center eastward to the central US. From days −2 to 0 (Fig. 4b, c), the positive feature spreads to encompass a greater portion of the Arctic while its southward extension moves to western North America. To the southeast, the negative height anomaly deepens, migrates to the eastern US and develops a more circular signature. During this time, Rossby wave energy flows into the negative height anomaly feature and is subsequently exported southeastward to the North Atlantic. By day 2 (Fig. 4d), the latter Rossby wave energy export has weakened the negative height anomaly over the eastern US which is also displaced eastward to the North American coast. At the same time, the upstream positive height anomaly has weakened and begun to break apart. The planetary scale component of the anomaly pattern (center column) largely resembles the negative phase of the NAM with modest negative height anomalies over the eastern US, thus directly contributing to the negative anomaly feature observed in this region. The planetary wave pattern amplifies in the days prior to ECW onset, and then weakens immediately afterward. In contrast, the synoptic scale pattern (right column) initially (Day −4; Fig. 4i) exhibits a zonal wave train signature from the subtropical North Pacific eastward to Canada. Notably, the anomalies over the northwestern Pacific and eastern North America are in phase with the planetary-scale anomalies and largely comprise the eastward propagating Rossby wave observed in the total anomaly field (Fig. 4a). The associated negative anomaly feature over Canada is elongated from northwest to southeast. In comparison to the climatological-mean dilatation structure analyzed by

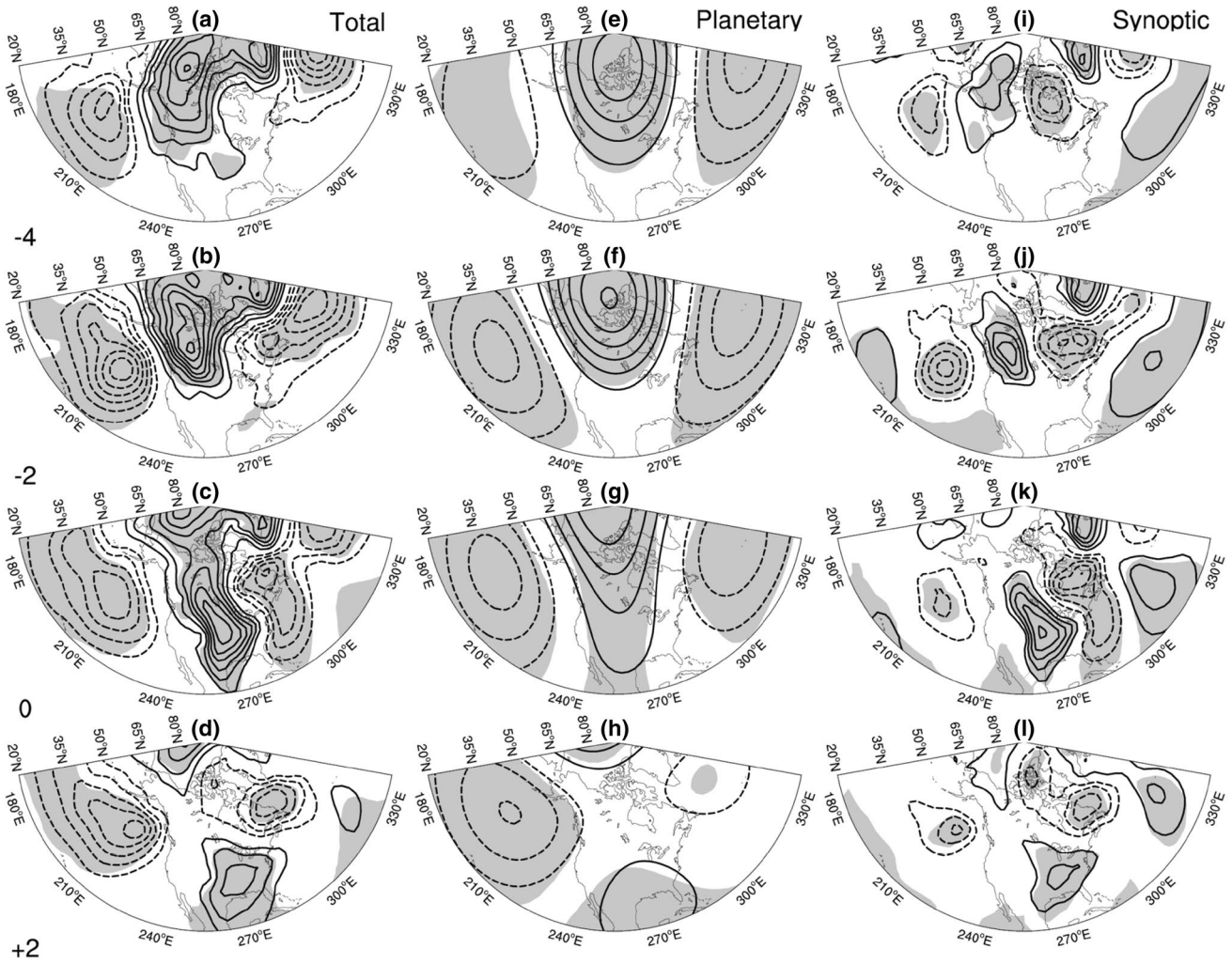

Fig. 3 Composite daily evolution of total SLP anomalies of the SE-ECW events for days **a** −4, **b** −2, **c** 0, and **d** +2 relative to the peak time. Contours are drawn for every 2 hPa. Shaded indicates that composite anomalies are statistically significant at 95% confidence. **e**–**h** As per **a**–**d**, but for planetary component of SLP anomalies. **i**–**h** As per **a**–**m**, but for synoptic component of SLP anomalies

Black and Dole (2000), the planetary-scale negative NAM structure acts to displace the midlatitude jet southward and increases the dilatation amplitude poleward of the Jet. From day −2 to 0 (Fig. 4j, k), the wave train propagates southeastward leading to a positive anomaly over the southwest and a deepened negative height anomaly over the eastern US. The southeastward moving negative anomaly is increasingly in phase with the pre-existing planetary anomaly. During this time, the negative height anomaly moves into a region of background (planetary) northeast-southwest stretching and becomes more circular (recalling its initial northwest to southeast elongation). By day 2 (Fig. 4l), the wave train has considerably weakened and propagated further eastward. The negative height anomaly over eastern North America is weakened and has attained a northeast-southwest elongation. The apparent planetary-scale deformation of the negative anomaly feature indicates that barotropic growth is likely a primary contributor to the short-term amplification of this upper level feature.

The composite SLP and Z300 anomaly lifecycle are in generally good agreement with prior ECW studies (e.g., Konrad 1996; Walsh et al. 2001; Westby and Black 2015). However, prior studies mainly focused on the circulation patterns over North America. Additionally, we provide a novel analysis of the separate evolution of planetary and synoptic-scale circulation components. Although Konrad (1996) noted this distinction, his results are based on linear lag correlations of planetary- and synoptic-scale circulations distinguished in terms of a nine-point Gaussian-type time filter with the intensity of the SE-ECW events. Such an approach presupposes a one-to-one relationship between lower frequencies and large spatial scales (versus the current approach that permits short-term variations in the planetary scale flow). In contrast, we analyze the composite lifecycle

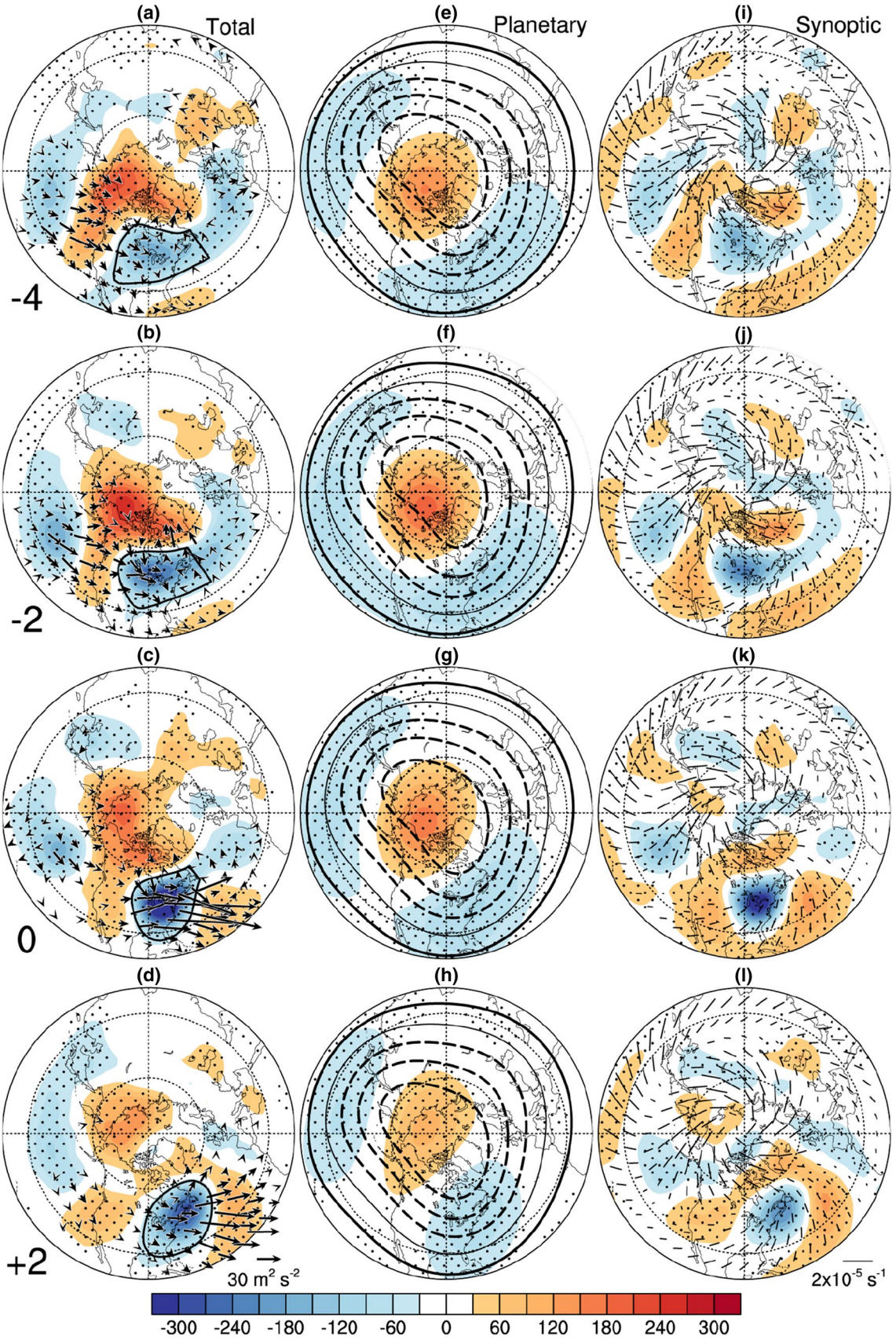
(a) Total
(e) Planetary
(i) Synoptic
-4
(b)
(f)
(j)
-2
(c)
(g)
(k)
0
(d)
(h)
(l)
+2
30 m² s⁻²
2x10⁻⁵ s⁻¹
-300 -240 -180 -120 -60 0 60 120 180 240 300

◂**Fig. 4** Composite daily 300 hPa geopotential height anomalies (Z300, shaded) and wave activity fluxes (arrows, $m^2\ s^{-2}$) of the SE-ECW events on days **a** −4, **b** −2, **c** 0, and **d** +2 relative to the peak time. Contours is −50 m which encloses negative height anomalies. Stippling indicates that composite anomalies are statistically significant at 95% confidence. **e**–**h** As per **a**–**d**, but for planetary component of Z300 anomalies. Contours represent the total field. **i**–**h** As per **a**–**m**, but for synoptic component of Z300 anomalies. The line segments denote axes of dilatation

of planetary- and synoptic-scale circulations isolated using a two-dimensional spherical harmonic analysis with no time filtering. Also, Westby and Black (2015) noted that ECW LMP circulations tend to be more stationary for ECWs concurrent with the negative phase of the NAO. Given that the SE-ECW events are concurrent with the negative NAM phase in the current paper, both planetary- and synoptic-scale circulations indeed exhibit more quasi-stationary compared to the counterparts studied by Konrad (1996).

As shown above, the evolution of the LMP, particularly the negative height anomaly feature over the southeastern US, coincides with ECW onset, consistent with Konrad and Colucci (1989) and Konrad (1996). Two questions naturally arise: how does the mid- to upper tropospheric LMP impact the surface wind and to what extent do the planetary- and synoptic waves respectively contribute to the surface wind anomaly. To address these questions, we perform a piecewise PV inversion in which the composite PV anomaly field is separated in terms of (a) different vertical levels and (b) planetary and synoptic spatial scales. After inversion, we then obtain the horizontal wind at 925 hPa, which is close to the surface. The results are displayed in Fig. 5 for Day −1, corresponding to the time of most rapid cold anomaly development over the region of interest. First considering the *observed* composite wind anomaly field (Fig. 5a), we note that anomalous northerlies prevail over the region extending from Hudson Bay via the Great Plains to the Gulf of Mexico, facilitating a southward advection of cold Canadian air into the southern US, consistent with Fig. 2. The corresponding 925 hPa wind anomaly pattern obtained from inverting the entire Day −1 PV anomaly field (Fig. 5b) closely resembles the observed wind anomaly pattern, helping to justify our use of piecewise PV inversion using the balance condition outlined in (6).

We next partition the composite PV anomaly field into upper level (500–100 hPa) and lower level (1000–600 hPa) pieces and obtain horizontal wind anomaly pattern related to each PV piece. The horizontal wind pattern induced by upper level PV anomalies exhibits a prominent cyclonic circulation centered over New England with prominent northerly flow extending through central North America. In contrast, the horizontal wind anomaly pattern due to lower PV anomalies is *qualitatively* anti-symmetric with respect to that due to the upper PV (Fig. 5d). Thus, we infer that the northerly wind anomaly causing ECW onset is dynamically induced by the middle and upper tropospheric components of the composite LMP, particularly the negative height anomaly feature located over the eastern US. We further partition the upper-level PV anomaly field into planetary and synoptic-scale components and perform additional PV inversions (Fig. 5e, f). The additional results reveal that the upper-level planetary PV anomaly feature induces northeasterly flow from northern Canada to the southwestern US, while the synoptic-scale PV anomaly is the primary contributor to the cyclonic anomaly found in Fig. 5c. Although the direct planetary wave contribution is small, it does help transport cold air from the Hudson Bay region toward central Canada and the upper Midwest, helping to feed the reservoir of cold air from which the ECW emanates. When the synoptic low deepens, the cold air is advected into the southeastern US.

Since the negative height anomaly feature over the eastern US is identified as the primary dynamical trigger of SE-ECW onset, it is of further interest to study the formation mechanisms for the negative height anomaly, itself, by applying the PTD methodology outlined in Eq. (11), which includes partitioning among, and scale interaction between, planetary- and synoptic-scale waves. Given that the cold SAT and negative height anomaly features are most robust on day 0, we first assess the spatial patterns of the various 300 hPa height tendency contributions just prior to onset (day −1; Fig. 6) and the respective contributions areal-averaged over the negative height anomaly (those anomalies enclosed by the −50 m contour displayed in Fig. 6) in Table 3. All the forcing terms from Eq. (11) are incorporated into this analysis and sum to the "net" value. First, we note a good quantitative agreement between the net forcing (Fig. 6h) and observed tendency (Fig. 6i) with a positive height tendency over the Great Plains and a negative height tendency over the eastern US. Differences between the net forcing and observed tendency come from (1) comparing an instantaneous tendency (RHS) with a finite-time difference (LHS), in which we use 6 hourly data and (2) the neglect of some subgrid-scale processes (Teubler and Riemer 2016). As anticipated in discussing Fig. 4, the contribution of term C closely resembles the net, indicating that Term C is a key dynamical forcing of LMP development (Fig. 6c). Term C includes both the translation and deformation of the synoptic wave by the background planetary-scale flow and furnishes 98.9% to the temporal change in the negative height anomaly at day −1. Baroclinic growth (Term B) plays an ancillary role in the LMP development as it provides a 16.5% contribution to the tendency pattern (Fig. 6b). Rossby wave retrogression (Term A) is roughly anti-symmetric to the net forcing pattern, providing an offsetting influence (~ −36.0%) upon the intensification of the negative height anomaly (Fig. 6a). Terms D (synoptic-scale nonlinearity),

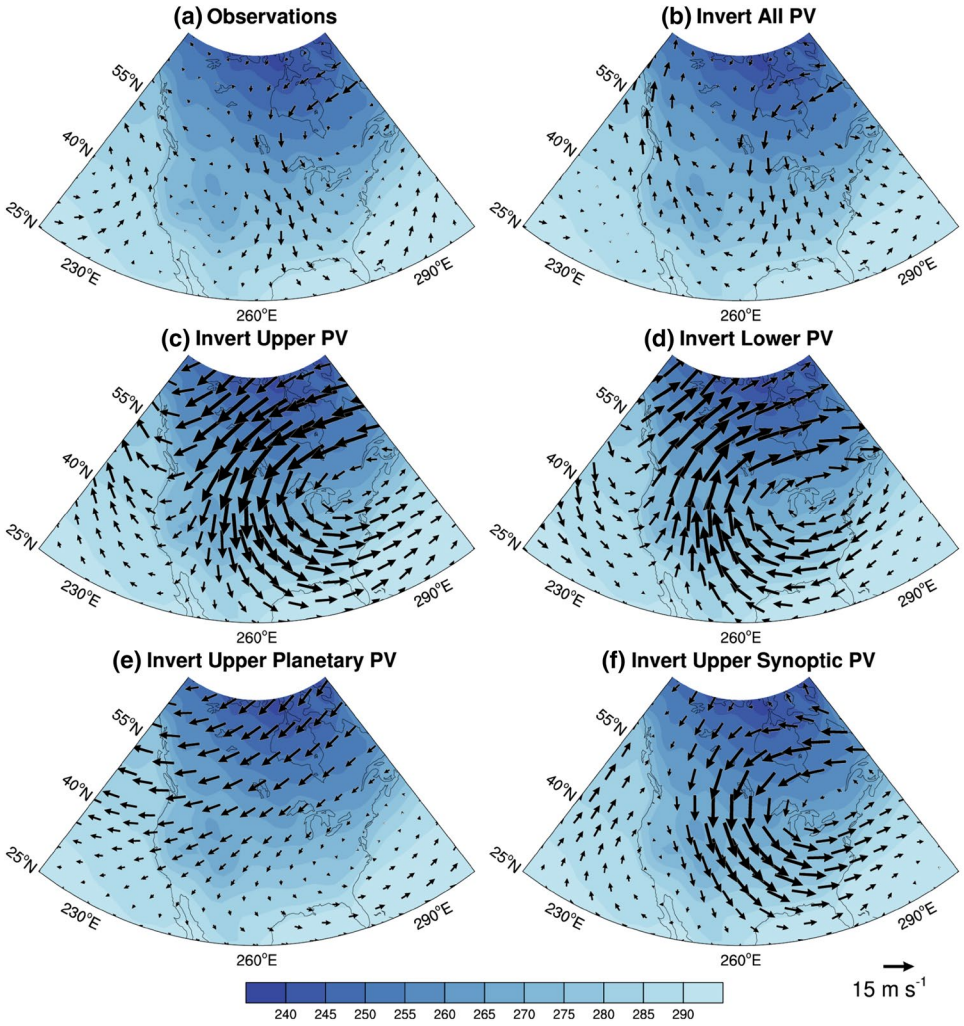

Fig. 5 A dynamical breakdown (in terms of PV) of the 925 hPa horizontal wind anomaly field (arrows; m s^{-1}) and climatological mean air temperature (shaded; K) on day − 1. The observed winds are displayed in **a**. **b** Displays winds due to the entire PV anomaly field while subcomponents due to individual PV anomaly "pieces" are displayed in **c**–**f** along with representative PV anomaly structures. Shown are wind anomaly pieces due to **c** upper PV, **d** lower PV, **e** upper planetary PV and **f** upper synoptic PV

P (planetary-scale nonlinearity) and the collective ageostrophic forcing are generally weaker and only provide minor contributions to LMP development (Fig. 6d, e, g). Finally, there is a weak offsetting contribution from term E (diabatic heating, Fig. 6f).

To assess the time evolution of the dynamical contributions to the traveling negative height anomaly, we track (in a Lagrangian manner) the distribution of grid points lying within the − 50 m contour encompassing the negative height anomaly for each day in the composite evolution. We then apply the PTD diagnosis to the height tendency pattern enclosed by this contour on each day (i.e., we are repeating the diagnostic analysis presented in Fig. 6 for each day in the composite evolution, but over a time-varying areal domain that is dependent on the extent and movement of the negative height anomaly feature). Figure 7 shows the resulting time series of areal-averaged PTD contributions to the height anomaly tendency during the composite life cycle of SE-ECW onset. Event intensity is defined as the average perturbation height anomaly within the contour of -50 m as shown in Figs. 4 and 6. Thus, for each day, we identify the contribution of each forcing term to the height tendency occurring within the negative height anomaly feature. Using Fig. 7, a quantitative measure of the respective contributions of the different terms in Eq. (11) to growth and decline can be assessed. We note that the net forcing is generally in good agreement with the actual height tendencies except for an overall underestimation prior to day − 1. As inferred from Fig. 6c, term C (the translation and deformation of the synoptic wave by the planetary-scale flow) is the main contributor to the intensification of the incipient and mature negative height anomaly (noting that a negative height tendency implies *intensification*). Term B (baroclinic growth) also provides a positive contribution to anomaly growth throughout the life cycle. Terms P (planetary nonlinearity) and agostrophic forcing provide weak strengthening during incipient and mature periods and thereafter weakly damp the negative height anomaly. Term D (synoptic nonlinearity) provides a negligible contribution until after onset when it acts to weaken the LMP. The Rossby wave propagation

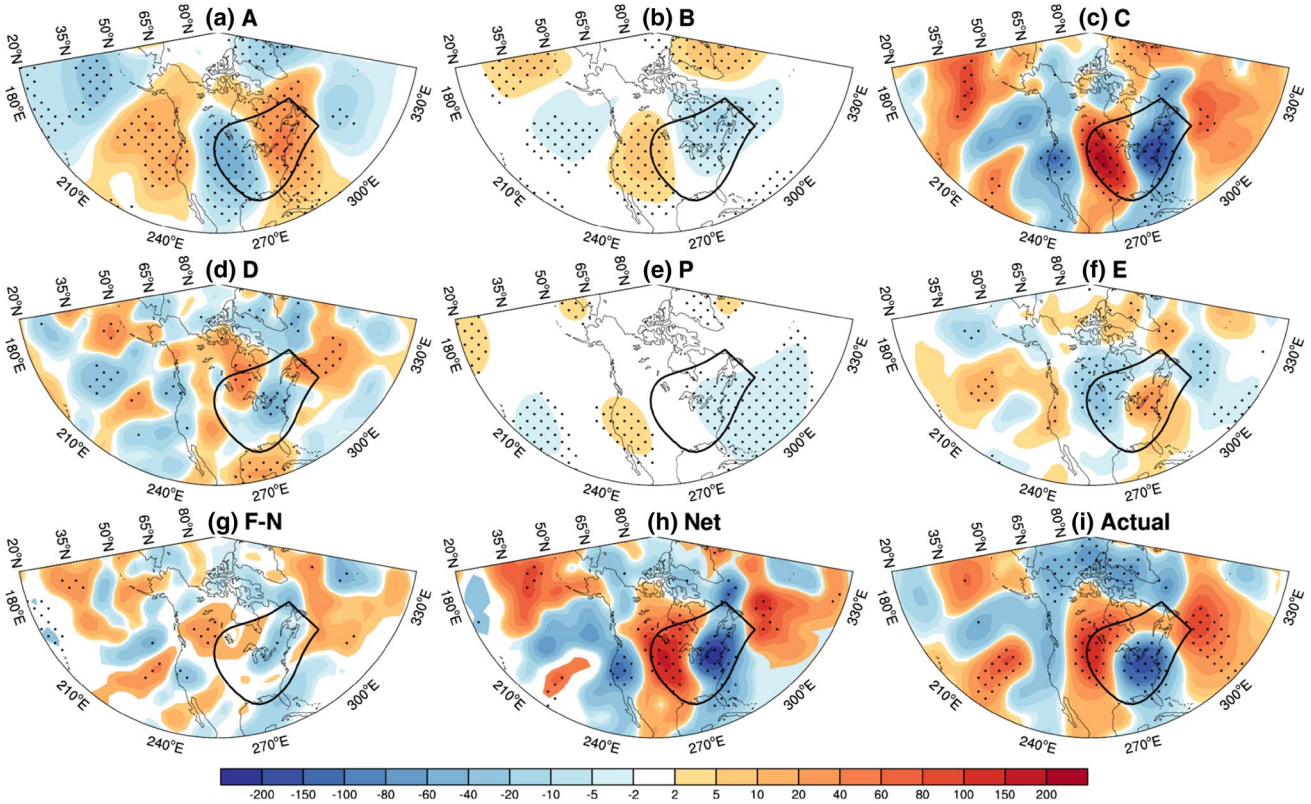

Fig. 6 300 hPa height change due to inverted forcing terms in Eq. (11): **a** term A; **b** term B; **c** term C; **d** term D; **e** term P; **f** term E; **g** sum of terms F-N; **h** net; and **i** actual. The stippling indicates composite height tendency anomaly values that are significant at the 95% confidence level. The contours represent those anomalies enclosed by −50 m

term (Term A) consistently opposes anomaly growth, consistent with Rossby wave energy propagating away from the negative height anomaly (Fig. 3c). The diabatic heating is negligible prior to Day 0 and thereafter helps sustain the (decaying) negative height anomaly.

The physical role of the respective linear PV advection terms is clarified by overlaying the corresponding wind vectors and PV fields for each, as is displayed in Fig. 8. The components of Term A (Rossby wave retrogression), are shown in Fig. 8a with the 300-hPa geostrophic winds associated with the *upper-level* synoptic PV anomalies overlying the planetary wave flow. The cyclonic circulation anomaly induced by upper-level synoptic PV advects high-PV (low-PV) air southward (northward) to the west (east), thereby locally inducing height falls (rises) and an overall tendency to move the synoptic wave pattern westward (opposing the eastward translation by the background planetary flow; Term C). We also note a weak cyclonic wind anomaly over the North Pacific associated with height falls (rises) over the central North Pacific (eastern North Pacific). The format of Fig. 8b follows that of Fig. 8a except that the vectors represent the 300-hPa geostrophic winds due to *lower-level* synoptic PV anomalies (i.e., encompassing Term B and baroclinic growth). The developing near-surface cold anomaly (e.g., Fig. 2b, c) induces a robust anticyclonic wind anomaly over North America that extends coherently upward to the 300-hPa level. The resulting southward advection of high PV air by the northerly flow over eastern North America encompasses a substantial portion of the negative height anomaly feature, leading to an overall magnitude amplification of the feature of interest.

This also contrasts with Nielsen-Gammon and Lefevre (1996), where baroclinic growth is only observed in association with a favorable vertical height anomaly tilt. As discussed above, the negative NAM-like planetary pattern induces near surface northerly flow leading to a cold air anomaly accumulation over central Canada. The resulting surface cold anomaly then contributes to the amplification of the upper-level negative height anomaly throughout its lifecycle. Figure 8 displays the components of Term C with the upper-level synoptic-scale PV anomalies overlying the climatological mean planetary flow. The PV anomaly is situated within a jet entrance region characterized by confluent flow. The net impact of this configuration is that the mean planetary-scale deformation field acts to make the synoptic-scale PV anomaly horizontally isotropic (round) via

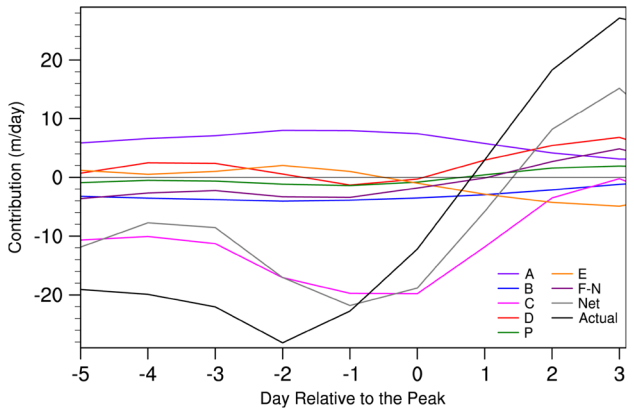

Fig. 7 Contribution from calculated forcing to the height tendency averaged within the region of the negative height anomaly shown in Figs. 4 and 6

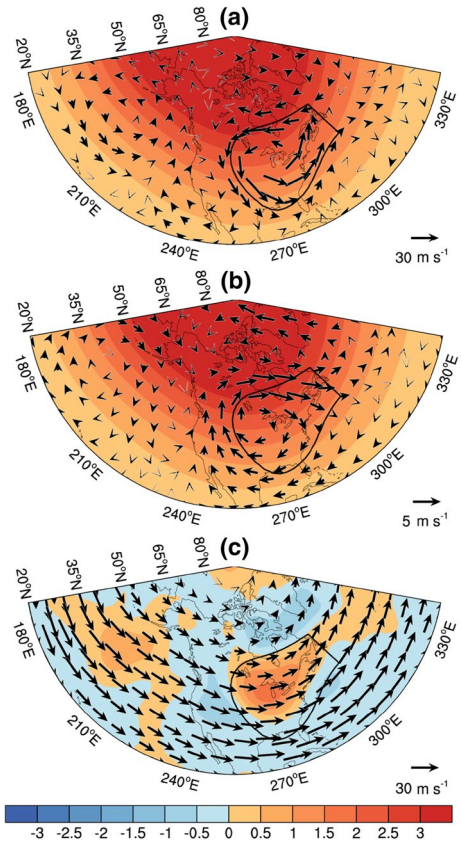

Fig. 8 Wind vector overlaying the upper-level PV field for terms **a** A, **b** B, and **c** C in Eq. (11) at 300 hPa on day − 1

northeast-southwestward stretching (Fig. 4j, k) suggesting that horizontal deformation is a potential growth mechanism during this period. To test this idea, we partition the planetary-scale flow into (i) a four-dimensional average (including time mean), (ii) a vertical average of the remaining three-dimensional variability and (iii) a residual, similar to Evans and Black (2003). Consistent with the results of their study, we find that the primary contributor to term C is the horizontal deformation of synoptic PV anomaly.

3.3 The NW-ECW events

A parallel composite diagnostic analysis of NW-ECW events is provided in this section with Figs. 9 and 10 displaying, respectively, the composite evolution of Z300 anomalies and time series of areal-averaged PTD contributions to the negative height tendency. In comparison with SE-ECW events, NW-ECW events feature an approximately quasi-stationary cold SAT anomaly with a regional feature that mainly extends over the northwestern US and western Canada (not shown). In addition, the cold anomaly pattern of NW-ECW events is less persistent than its SE-ECW counterpart. Unlike the SE-ECW events, characterized by meridionally-elongated SLP anomalies, the NW-ECW cases exhibit zonally-oriented SLP anomalies. Although the positive anomaly feature includes a southward extension, the primary center over the Gulf of Alaska is quasi-stationary. The planetary-scale SLP anomalies of NW-ECW events provide a considerably greater contribution to the total SLP anomaly field than found for SE-ECW events. The synoptic-scale component is relatively quasi-stationary and closely follows the total anomaly field, noting that the amplitude of the positive height anomaly center is weaker.

In contrast to the SE-ECW events, at upper levels a positive height anomaly is centered over the Gulf of Alaska with distinct Rossby wave energy export to the southeast into an intensifying downstream negative height anomaly feature extending from western North America to Greenland (Fig. 9a–d). The positive height anomaly retrogresses westward to the Chukchi Peninsula, while the downstream negative height anomaly deepens with an increasing southwest–northeast anomaly orientation over the northwestern US. Considering the planetary wave anomaly structure (Fig. 9e–h), we observe that the pattern, which combines aspects of the negative WP and positive NAO patterns, provides a more important direct contribution to the total anomaly field than its SE-ECW counterpart. There is a gradual westward movement of the planetary-scale pattern as the positive height anomaly over the Bering Strait strengthens and retrogresses westward to northeastern Asia. In contrast to the SE-ECW events, the synoptic-scale wave train (Fig. 9i–l) gradually comes into phase with the planetary scale pattern as it travels from the North Pacific to the US. As shown in Xie et al. (2017b), the sixth planetary wave pattern tends to weaken the jet core over the North Pacific, where the zonal wind decelerates, while the zonal wind accelerates over North America. As a result, the zonal wind gradient increases over the western coast of North America, which increases the zonal deformation and decreases the

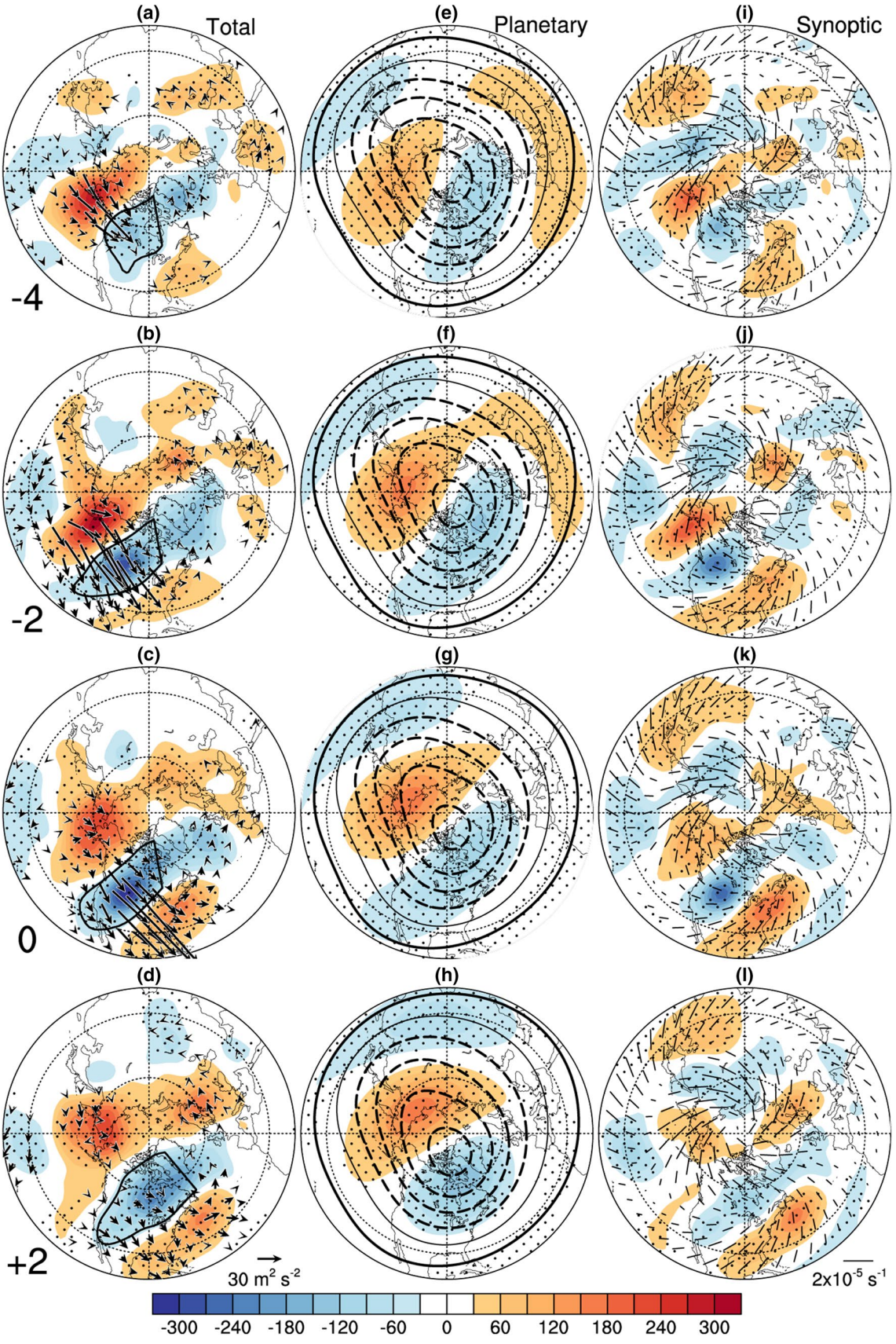

Fig. 9 As in Fig. 4, but for the NW-ECW events

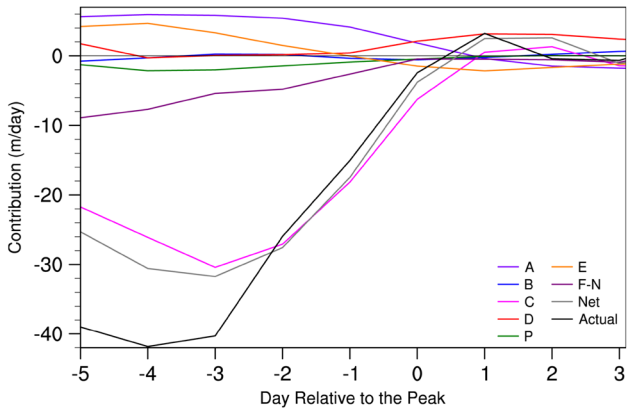

Fig. 10 As in Fig. 7, but for the NW-ECW events

angle of dilatation axis. The negative height anomaly exhibits southwest–northeast orientation and is orthogonal to the strengthened dilatation axis over the western US, indicating a significant potential for barotropic deformation.

Although both synoptic and planetary scale upper PV contribute to near-surface northerly wind anomalies along the west coastline, it is the planetary-scale contribution that most consistently provides northerly flow over the interior portions of western North America (not shown). This is unlike SE-ECW events (Fig. 5) for which upper tropospheric synoptic-scale features provided the dominant proximate source of northerly flow enacting ECW onset.

Figure 10 shows the resulting time series of areal-averaged PTD contributions to the height anomaly tendency during the composite life cycle of NW-ECW onset (see discussion of Fig. 7 for further details). There is again a good correspondence between the actual height tendencies for each day and the net forcing (RHS of (7)). In comparison with the SE-ECW PTD analysis (Fig. 7), the incipient height falls during NW-ECW events are more dramatic. The difference is mainly due to Term C (see also Table 3), especially the horizontal deformation of synoptic waves by the planetary scale flow (not shown), noting the dilatation axes are orthogonal to the eddy major axis of the incipient negative anomaly for NW-ECW events. In comparison with SE-ECW events, the contributions from term F-N and P are more evident in the incipient stages of NW-ECW events. Terms B (baroclinic growth) and D (synoptic nonlinearity) provide negligible contributions. The offsetting contributions of Terms A (Rossby wave retrogression) and E (diabatic heating) gradually decrease over time. Compared to SE-ECW events, there is a greater cancelation between the forcing tendency couplet within the negative height anomaly region, observed in Terms A and particularly B, leading to a weaker positive offsetting contribution (Fig. 10; Table 3). Unlike SE-ECW events, the positive SLP anomaly feature over western North America is sandwiched between negative anomalies to the north and south for NW-ECW events. Therefore, the strength and latitudinal extent of anomalous northerly flow over the Great Lakes is weaker than the southerlies associated with low level PV anomalies (not shown), resulting in a strong cancellation between negative and positive PV advection in the lower troposphere.

4 Summary and discussion

In this study, we have investigated the composite intraseasonal evolution of wintertime SE- and NW-ECW events, each separately linked to distinct planetary wave patterns, for the period of 1950–2005. The SE-ECW events are more frequent during the negative phase of a NAM-like planetary wave pattern while NW-ECW events tend to recur during a planetary wave pattern that combines the negative phase of the WP with the positive phase of the NAO. The respective composite circulation anomalies for each of the two event types are decomposed into planetary- and synoptic-scale components and their individual signatures and contributions toward ECW onset are reviewed. By application of quasigeostrophic piecewise tendency diagnosis (PTD), we further examine the dynamical roles of, and interactions between, planetary and synoptic features in the formation and intensification of the large-scale meteorological patterns (LMP) that induce ECW onset.

Planetary-scale and synoptic-scale waves jointly act to produce ECW events. First, ECW events tend to occur within a favorable background environment provided by direct contributions from the planetary wave field. Second, the background planetary wave circulation anomaly helps foster synoptic-scale anomaly growth via enhanced regional dynamical scale interaction, mainly via planetary-scale alterations in the barotropic deformation. Considering SE-ECW events, the planetary scale pattern most closely resembling the negative phase of NAM/AO provides a sizable contribution to the total wave pattern, helping induce northwesterly flow that transports cold air into the incipient regional

Table 3 Percent contribution by each term in Eq. (11) to the negative height anomaly at day −1

	A	B	C	D	P	E	F-N
SE	−36.0	16.5	98.9	5.9	7.0	−6.6	14.4
NW	−26.4	2.8	102.6	2.7	5.5	−1.6	14.4

reservoir of cold air for the ECW. As a synoptic wave train propagates eastward, the planetary wave pattern serves to deepen the embedded negative height anomaly (key to ECW onset) via barotropic deformation and baroclinic growth. On the one hand, the NAM-like planetary-wave structure leads to a southward displacement of the extratropical jet, resulting in a planetary-scale deformation field with a dilatation axis extending from northwest-southeast (northeast–southwest) poleward (equatorward) of the Great Lakes. Since the major axis of the incipient negative synoptic-scale height anomaly extends from northwest to southeast, it becomes barotropically deformed by the background planetary-scale flow into a more isotropic (round) anomaly structure by the time of onset (day 0). In addition, however, the surface cold anomalies translated by both the planetary and synoptic waves provide a secondary feedback role in intensifying the upper level trough (via baroclinic growth). Ageostrophic forcing also provides a secondary contribution toward anomaly growth while Rossby wave retrogression provides a substantial damping of the negative height anomaly.

In comparison to SE-ECW events, the planetary-scale dynamical features provide a more important direct contribution to the anomalous circulation enacting NW-ECW onset in both SLP and upper level height fields. As a consequence, the resulting cold anomaly exhibits greater quasi-stationary behavior as it magnifies over the northwestern US. The planetary wave structure results in a strongly intensified background barotropic deformation field, in which the dilatation axes are perpendicular to the northeast–southwest oriented major axis of the synoptic-scale negative height anomaly. PTD analysis verifies that barotropic deformation robustly contributes to the growth of the key upper level trough feature. In contrast to SE-ECW events, the lower tropospheric synoptic scale anomaly is meridionally restricted leading to negligible baroclinic feedback upon the upper level trough. Instead, ageostrophic forcing plays a greater secondary role in deepening the negative height anomaly.

Xie et al. (2017a, b) separately identified (a) three ECW patterns and their associated LMPs and (b) six planetary wave patterns and their association with ECWs. They noted that ECWs preferentially occur during episodes of the fourth and six planetary wave patterns. However, the underlying dynamical processes leading to the formation and maintenance of responsible LMPs were not explored, particularly the interplay of planetary and synoptic waves. Noting that LMPs are comprised of both planetary waves and synoptic waves, this paper decomposes the LMP into planetary and synoptic-scale components and determines their individual direct contributions to the total wave field as well as the planetary-scale influence upon the synoptic waves. The unique new contribution of this paper is in characterizing the physical manner in which planetary waves and synoptic waves *jointly* work together to initiate ECW events. Notably, the planetary waves not only provide a direct contribution to circulation field enacting ECW events but also alter the background circulation field in such a manner that promotes synoptic waves growth via increases in regional barotropic deformation. This finding is in contrast to prior studies (e.g., Konrad 1996; Nielsen-Gammon and Lefevre 1996; Evans and Black 2003; Francis and Vavrus 2012, 2015) mainly focusing on the separate, individual roles of planetary waves. Konrad (1996) noted a direct contribution of the planetary-scale circulation to total fields, while Nielsen-Gammon and Lefevre (1996) and Evans and Black (2003) concentrated on the role of climatological mean or large-scale background circulations in forming mobile trough or persistent flow anomalies. Francis and Vavrus (2012, 2015) found that a weakened jet decelerates the eastward progression of ridges and troughs, which increases the likelihood of persistent weather patterns and extreme events. In contrast, we find that ECW events preferentially occur in planetary wave patterns that simultaneously provide a direct contribution to the responsible circulation field as well as a favorable barotropic deformation background that amplifies the synoptic-scale negative height anomaly helping to enact ECW onset. In our study, a decelerated progression of ridges and troughs is not observed in either SE and NW-ECW events.

There has been a decadal variation in SE-ECW frequency, consistent with a climate impact upon ECW events. As evident from Table 1, most SE-ECW events occurred in 1960s (roughly 8 events), mid-1970s to mid-1980 (6 events) and 2000s (7 events), which correspond to an earlier cooler climate phase and the global warming hiatus (IPCC 2012). During these periods, there is a higher population distribution of negative NAM-like patterns (Fig. 5d of Xie et al. 2017b). Xie et al. (2017a) showed that low Arctic sea ice extent and high Eurasian snow cover extent are linked to increases in SE-ECW frequency. It could be possible that both low Arctic sea ice extent and high Eurasian snow cover extent help force more frequent episodes of the fourth planetary wave pattern, which resembles the negative phase of NAM, and thus are linked to a higher frequency of SE-ECWs. Our future research will attempt to explore these linkages in greater detail.

This study has mainly focused on the dynamical forcing of the upper-level negative height anomaly features implicated in inducing ECW onset. Since these upper-level trough features are mainly synoptic-scale in structure, we have implicitly provided a greater focus on the dynamical forcing of the synoptic-scale anomalies than assessing the proximate sources for corresponding planetary scale anomalies. Also, we have purposely chosen to focus on two particular types of ECW events due to their relationship to commonly recognized teleconnection patterns. Future research efforts will be expanded to include a consideration of other categories of ECW events as well as an exploration of the dynamical forcing of the associated planetary-scale wave field.

Acknowledgements The authors are grateful to two anonymous reviewers for their constructive and helpful comments. This work was supported by the U.S. Department of Energy, Office of Biological and Environmental Research, Awards DE-SC0012554. Yi Deng is also partly supported by the National Science Foundation Climate and Large-Scale Dynamics (CLD) program through Grants AGS-1354402 and AGS-1445956. Zuowei Xie is also partly supported by National Natural Science Foundation of China through Grants 41875078 and 41630424. The authors thank writers of the NCAR Command Language (UCAR/NCAR/CISL/TDD 2018), which is employed to plot the figures.

References

Baxter S, Nigam S (2015) Key role of the North Pacific Oscillation–West Pacific Pattern in generating the extreme 2013/14 North American Winter. J Clim 28:8109–8117. https://doi.org/10.1175/JCLI-D-14-00726.1

Black RX, Dole RM (2000) Storm tracks and barotropic deformation in climate models. J Clim 13:2712–2728

Branstator G (2002) Circumglobal teleconnections, the jet stream waveguide, and the North Atlantic Oscillation. J Clim 15:1893–1910

Cellitti MP, Walsh JE, Rauber RM, Portis DH (2006) Extreme cold air outbreaks over the United States, the polar vortex, and the large-scale circulation. J Geophy Res 111:D02114. https://doi.org/10.1029/2005JD006273

Cohen J, Screen JA, Furtado JC, Barlow M, Whittleston D, Coumou D, Francis J, Dethloff K, Entekhabi D, Overland J, Justin J (2014) Recent Arctic amplification and extreme mid-latitude weather. Nature Geosci 7:627–637. https://doi.org/10.1038/ngeo2234

Evans KJ, Black RX (2003) Piecewise tendency diagnosis of weather regime transitions. J Atmos Sci 60:1941–1959

Francis JA, Vavrus SJ (2012) Evidence linking Arctic amplification to extreme weather in mid-latitudes. Geophy Res Lett. https://doi.org/10.1029/2012GL051000

Francis JA, Vavrus SJ (2015) Evidence for a wavier jet stream in response to rapid Arctic warming. Environ Res Lett 10(1):14005

Grotjahn R, Black R, Leung R, Wehner MF, Barlow M, Bosilovich M, Gershunov A, Gutowski WJ Jr, Gyakum JR, Katz RW, Lee YY, Lim YK, Prabhat (2015) North American extreme temperature events and related large scale meteorological patterns: a review of statistical methods, dynamics, modeling, and trends. Clim Dyn 46:1151–1184. https://doi.org/10.1007/s00382-015-2638-6

Harnik N, Messori G, Caballero R, Feldstein SB (2016) The Circumglobal North American wave pattern and its relation to cold events in eastern North America. Geophys Res Lett 43:11015–11023

IPCC (2012) Managing the risks of extreme events and disasters to advance climate change adaptation. In: Field CB, Barros V, Stocker TF, Qin D, Dokken DJ, Ebi KL, Mastrandrea MD, Mach KJ, Plattner GK, Allen SK, Tignor M, Midgley PM (eds) A special report of working groups i and ii of the intergovernmental panel on climate change. Cambridge University Press, Cambridge

Jiang T, Deng Y, Li W (2013) Local kinetic energy budget of high-frequency and intermediate-frequency eddies: winter climatology and interannual variability. Clim Dyn 41:961–976

Kalnay E, Kanamitsu M, Kistler R, Collins W, Deaven D, Gandin L, Iredell M, Saha S, White G, Woollen J, Zhu Y, Chelliah M, Ebisuzaki W, Higgins W, Janowiak J, Mo KC, Ropelewski C, Wang J, Leetmaa A, Reynolds R, Jenne R, Joseph D (1996) The NCEP/NCAR 40-year reanalysis project. Bull Am Meteorol Soc 77:437–471

Kolstad EW, Breiteig T, Scaife AA (2010) The association between stratospheric weak polar vortex events and cold air outbreaks in the Northern Hemisphere. Q J R Meteorol Soc 136:886–893

Konrad CEII (1996) Relationships between the intensity of cold-air outbreaks and the evolution of synoptic and planetary-scale features over North America. Mon Weather Rev 124:1067–1083

Konrad CEII (1998) Persistent planetary scale circulation patterns and their relationship with cold air outbreak activity over the eastern United States. Int J Climatol 18:1209–1221

Konrad CEII, Colucci SJ (1989) An examination of extreme cold air outbreaks over eastern North America. Mon Weather Rev 117:2687–2700

Loikith PC, Broccoli AJ (2012) Characteristics of observed atmospheric circulation patterns associated with temperature extremes over North America. J Clim 25:7266–7281. https://doi.org/10.1175/JCLI-D-11-00709.1

Loikith PC, Broccoli AJ (2014) The influence of recurrent modes of climate variability on the occurrence of winter and summer extreme temperatures over North America. J Clim 27:1600–1618

Mak MK, Cai M (1989) Local barotropic instability. J Atmos Sci 46:3289–3311

McDaniel BA, Black RX (2005) Intraseasonal dynamical evolution of the northern annular mode. J Clim 18:3820–3839

Messori G, Caballero R, Gaetani M (2016) On cold spells in North America and storminess in western Europe. Geophys Res Lett 43:6620–6628

Nakamura H, Nakamura M, Anderson JL (1997) The role of high- and low-frequency dynamics in blocking formation. Mon Weather Rev 125:2074–2093

Nielsen-Gammon JW, Lefevre RJ (1996) Piecewise tendency diagnosis of dynamical processes governing the development of an upper-tropospheric mobile trough. J Atmos Sci 53:3120–3142

Takaya K, Nakamura H (2001) A formulation of a phase-Independent wave-activity flux for stationary and migratory quasigeostrophic eddies on a zonally varying basic flow. J Atmos Sci 58:608–627

Teubler F, Riemer M (2016) Dynamics of Rossby wave packets in a quantitative potential vorticity-potential temperature framework. J Atmos Sci 73(3):1063–1081

Thompson DWJ, Wallace JM (1998) The Arctic oscillation signature in the wintertime geopotential height and temperature fields. Geophys Res Lett 25:1297–1300

Trenary L, Delsole T, Tippett MK et al (2015) Was the cold eastern US winter of 2014 due to increase variability? [in "Explaining Extremes of 2014 from a Climate Perspective"]. Bull Am Meteorol Soc 96(12):S15–S19

UCAR/NCAR/CISL/TDD (2018) The NCAR Command Language (Version 6.5.0) [Software]. UCAR/NCAR/CISL/TDD, Boulder, Colorado. https://doi.org/10.5065/D6WD3XH5

Walsh JE, Phillips AS, Portis DH, Chapman WL (2001) Extreme cold outbreaks in the United States and Europe, 1948–99. J Clim 14:2642–2658

Watt-Meyer O, Kushner P (2015) Standing and travelling wave contributions to the persistent ridge-trough over North America during winter 2013/14. In: American Geophysical Union 2015 Fall Meeting. 14–19 December 2015. https://agu.confex.com/agu/fm15/meetingapp.cgi/Paper/79553. Accessed 17 Dec 2015

Westby RM, Black RX (2015) Development of anomalous temperature regimes over the southeastern United States: synoptic behavior and role of low-frequency modes. Weather Forecast 30:553–570. https://doi.org/10.1175/WAF-D-14-00093.1

Westby RM, Lee YY, Black RX (2013) Anomalous temperature regimes during the cool season: long-term trends, low-frequency mode modulation, and representation in CMIP5 simulations. J Clim 26:9061–9076. https://doi.org/10.1175/JCLI-D-13-00003.1

Wilks DS (2006) Statistical methods in the atmospheric sciences, 2rd. Academic Press, Waltham

Xie Z, Black RX, Deng Y (2017a) The structure and large-scale organization of extreme cold waves over the conterminous United States. Clim Dyn 49:4075–4088. https://doi.org/10.1007/s00382-017-3564-6

Xie Z, Black RX, Deng Y (2017b) Daily-scale planetary wave patterns and the modulation of cold season weather in the northern extratropics. J Geophys Res Atmos 122:8383–8398. https://doi.org/10.1002/2017JD026768

Yanai M, Li C, Song Z (1992) Seasonal heating of the Tibetan Plateau and its effects on the evolution of the Asian summer monsoon. J Meteorol Soc Japan 70:319–351

Zeng QC (1983) The evolution of a Rossby-wave packet in a three-dimensional baroclinic atmosphere. J Atmos Sci 40(1):73–84